Microporous and Mesoporous Materials 338 (2022) 111960

Contents lists available at ScienceDirect

Microporous and Mesoporous Materials

journal homepage: www.elsevier.com/locate/micromeso

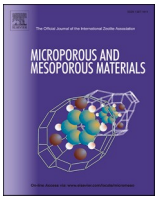

# Self-diffusion of mixed xylene isomers in ZIF-71 crystals dispersed in a polymer to form a hybrid membrane

Amineh Baniani [a], Matthew P. Rivera [b], Ryan P. Lively [b], Sergey Vasenkov [a,*]

[a] Department of Chemical Engineering, University of Florida, Gainesville, FL, 32611, USA
[b] School of Chemical & Biomolecular Engineering, Georgia Institute of Technology, Atlanta, GA, 30332, USA

ARTICLE INFO

*Keywords:*
Self-diffusion
PFG NMR
Mixed-matrix membranes
ZIF-71
Liquid separations

ABSTRACT

$^{13}$C pulsed field gradient (PFG) NMR was used to quantify self-diffusion of a *p*-xylene/*o*-xylene mixture inside zeolitic imidazolate framework-71 (ZIF-71) crystals dispersed in a Torlon polymer to form a ZIF-71/Torlon mixed-matrix membrane (MMM). The corresponding reference PFG NMR measurements with a bed of a loosely packed bed of ZIF-71 crystals were also performed. This study is motivated by a demonstrated potential of ZIF-based MMMs for liquid separations. Selective $^{13}$C isotopic labelling of each xylene isomer was used to ensure that the self-diffusivity of each isomer in the mixture is measured independently and correctly. The diffusion measurements were performed at different diffusion times at 296 K. The observed dependencies of intra-ZIF self-diffusivities in ZIF-71/Torlon MMMs and the corresponding ZIF-71 crystal beds on diffusion time were explained by an influence of the external crystal surface on the studied diffusion process. Analysis of the time dependencies of the self-diffusivities measured for each xylene isomer allowed obtaining intra-ZIF self-diffusivities not perturbed by crystal surface effects as well as the corresponding diffusion selectivity for the studied sorbate mixture. The reported selectivity of around 4 demonstrates promising separation behavior of the considered membrane type.

## 1. Introduction

Mixed-matrix membranes (MMMs), which are formed by dispersing porous filler particles in a polymeric matrix, have exhibited a superior separation capability than the pure polymeric membranes [1–12]. Hence, MMMs represent a promising membrane technology for energy-efficient gas and liquid separations. The enhanced separation properties of MMMs result from the molecular sieving and/or selective adsorption properties of filler particles integrated with the mechanical properties and scalability of pure polymers. Across a variety of different organic/inorganic fillers, zeolitic imidazolate frameworks (ZIFs) have demonstrated notable advantages related to their good chemical and thermal stabilities coupled with tunable pore sizes and/or apertures in the range of about 0.2–2.0 nm [13–15].

Many different types of ZIF-containing MMMs have been investigated for gas and/or liquid separations using simulation and experimental techniques (see, for example [10–12,16–24]). In particular, ZIF-71-based MMMs have been explored for separation of liquid sorbates exhibiting larger sizes than light gas molecules [25–27]. ZIF-71 is composed of fully coordinated Zn metal centers and dichloromidazole ligands with a crystallographic pore aperture of 4.2 Å [13]. This aperture size, which is larger than those of many other well-studied ZIFs, such as ZIF-8, makes ZIF-71 attractive for molecular sieving of liquid sorbates exhibiting molecular sizes larger than those of light gases including carbon dioxide and methane.

The diffusion process through MMMs is rather complex because diffusivities are usually different in the various MMM components (i.e. polymer and filler). As a result, microscopic diffusion measurements performed selectively for a particular MMM component are needed in addition to conventional macroscopic measurements through the entire membrane for a better quantification and understanding of the MMM diffusion process. In particular, quantifying diffusion inside a ZIF component of MMMs is important as transport properties of this component can change due to confinement in a polymer [12,28–32]. Until now, such changes were directly observed only for a diffusion of gas molecules [28–30]. In addition to PFG NMR, other microscopic experimental techniques including infrared microscopy (IRM) and interference microscopy (IFM) have demonstrated the capability to measure diffusion inside microporous crystals, such as zeolite and ZIF crystals [33–36]. However, IRM and IFM are not expected to be suitable

* Corresponding author.
*E-mail address:* svasenkov@che.ufl.edu (S. Vasenkov).

https://doi.org/10.1016/j.micromeso.2022.111960
Received 24 February 2022; Received in revised form 15 April 2022; Accepted 2 May 2022
Available online 10 May 2022

for measurements of intra-crystalline diffusion in microporous crystals located inside MMMs. IRM and IFM techniques rely on the measurements of the IR or visible light transmitted through a porous sample. For MMM samples, the polymer phase and more than a single crystal at different orientations are expected to contribute to the measured data. This significantly complicates the processing and interpretation of the measured data. In addition to measurements, molecular dynamics (MD) simulations can be used to study intra-crystalline diffusion [33].

In our recent work, we have demonstrated successful measurements of intra-ZIF diffusion in an MMM for a single component liquid using pulsed field gradient (PFG) NMR [37]. Since in separations more than one molecular component is typically present inside a membrane, it is important to have an ability of quantifying diffusion for liquid mixtures in MMMs. Motivated by this consideration, in the present work we expanded our recent study of an intra-ZIF diffusion inside MMM [37] to a two component mixture. A *p*-xylene/*o*-xylene mixture, which is relevant for separation applications, was selected. Diffusion studies were carried out at 296 K using the $^{13}$C PFG NMR at 17.6 T and large magnetic field gradients (up to 23 T/m) in a way allowing separate diffusion measurement for each molecular component in the mixture. To our knowledge, this work represents the first report on quantifying diffusion of mixed liquid sorbates inside porous filler particles confined in MMMs.

## 2. Experimental

### 2.1. Preparation of ZIF-71

ZIF-71 was prepared following a modified version of a previous synthesis procedure [38]. 0.585 g of zinc acetate dehydrate (2.67 mmol) was dissolved in 100 mL of methanol. Separately, 1.461 g of 4,5-dichloroimidazole (10.67 mmol) was dissolved in 100 mL of methanol. 0.581 g of imidazole (8.53 mmol, 0.8 equivalents relative to 4,5-dichloroimidazole) was added to the 4,5-dichloroimidazole solution and dissolved with sonication. The two solutions were combined and allowed to sit undisturbed at room temperature for two days. The product was isolated by centrifugation. This product was washed with *N*-methyl-2--pyrrolidone (NMP) for three days, replacing with fresh NMP each day by decanting without centrifugation. The large ZIF crystals were then washed with methanol for three days, replacing with fresh methanol each day, and dried at 383 K under vacuum overnight. Fig. S1 shows scanning electron microscopy (SEM) images of ZIF-71 crystals and of the corresponding mixed matrix membrane discussed below. Fig. S2 presents the crystal size distribution, which was determined by analyzing SEM images in the image processing software ImageJ and measuring the size of ~100 randomly selected crystals. The powder x-ray diffraction patterns are presented in Fig. S3. Despite a minor shift to the right, the pattern shows good consistency with the predicted one from literature (Fig. S3). The ZIF surface area was investigated with $N_2$ physisorption on a Quadrasorb from Anton-Parr (Fig. S4). The BET surface area was found to be slightly lower than in the previous report [38]. This decreased surface area is likely due to some of the modulating linker remaining trapped within the framework; however, the crystals still maintain a high surface area of over 650 $m^2/g$.

### 2.2. ZIF-71/Torlon MMM synthesis

0.7 g of ZIF-71 and 0.3 g of dried Torlon were dissolved in 5.6 g NMP. The mixture was placed on a rolling mixer under a heat lamp (creating an ambient temperature of ~328 K) until complete polymer dissolution, usually 1–2 days. The mixture was sonicated 10 times in 30 s intervals with a Branson Digital Sonifier set at 30% amplitude, with approximately 1 min between sonications. A clean glass plate was heated on a hot plate set to 393 K in a fume hood. The dope was cast on the glass plate using the film casting technique and a 10 mil casting knife. The resulting film was allowed to dry on the plate overnight. The film was peeled off the plate and washed with methanol for three days, replacing with fresh methanol each day. The film was then dried at 383 K under vacuum overnight. No noticeable defects were observed in the MMM sample by SEM (Fig. S1B). Fig. S5 shows a comparison of the MMM and neat ZIF powder XRD patterns. The patterns show good agreement, suggesting that the ZIF filler is present in the membrane and maintains its crystal structure throughout the membrane fabrication process.

### 2.3. Preparation of NMR samples

The PFG NMR samples were prepared in a similar way as described in Ref. [37]. The tightly packed strips of ZIF-71/Torlon MMM with a height of about 30 ± 5 mm were inserted into 5 mm NMR tubes (Wilmad Labglass, Inc.). Similarly, ZIF-71 crystals were packed inside 5 mm NMR tubes to reach a height of about 20 ± 5 mm. The samples were attached to a custom-made vacuum system to degas overnight at 373 K before sorbate loading. After degassing, the samples with the MMM or ZIF-71 crystal bed were loaded with an approximately equimolar mixture of two xylene isomers, i.e. *p*-xylene and *o*-xylene. Some samples were prepared with both isomers to be $^{13}$C-labeled: 99% isotopic purity $^{13}C_2$-labeled *p*-xylene (Sigma-Aldrich), and 99% isotopic purity $^{13}C_2$-labeled *o*-xylene (Sigma-Aldrich). A fraction of the samples was prepared with one unlabeled isomer, i.e. *p*-xylene (Sigma-Aldrich) or *o*-xylene (Sigma-Aldrich), while the other isomer was $^{13}C_2$-labeled. The loading was carried out by cryogenically transferring into the NMR samples the desired amounts of the two xylene isomers using liquid nitrogen. After loading, the samples were flame sealed and removed from the vacuum system. For all the samples, enough liquid sorbates were loaded to ensure the conditions of sorption equilibrium with the saturation vapor pressure of each sorbate.

Intra-ZIF xylene concentrations in the samples with ZIF-71 beds were estimated similarly as discussed in Ref. [37] for single components. Briefly, the total amount of each sorbate in the samples was estimated from the measured magnitude of the corresponding $^{13}$C NMR spectra (viz. the area under the spectrum). For these measurements we used identically prepared samples with the isomer mixtures where only one isomer was $^{13}$C labeled. Clearly, it can be assumed that for such samples only the labeled isomer was measured by $^{13}$C NMR. It is important to note that $^{13}$C labeled xylene molecules located inside and outside of ZIF-71 crystals contributed to the measured spectra. To estimate the intra-ZIF fraction of the signal, a difference between the $^{13}$C $T_2$ NMR relaxation times for the molecules located inside and outside the crystals was used. $^{13}$C $T_2$ NMR relaxation time measurements will be discussed below. In addition to the $T_2$ values inside and outside the crystals, these measurements also yielded the corresponding molecular fractions. For each $^{13}$C labeled xylene isomer, the intra-ZIF sorbate amount in a ZIF bed sample was estimated by multiplying the intra-ZIF component fraction form the $^{13}$C $T_2$ NMR relaxation measurements with the total amount of the sorbate in the sample. Table 1 shows the intra-ZIF concentration values at 296 K for the studied mixture. Owing to the procedure of sample loading, viz. sample equilibration with the sorbates at the saturation vapor pressures, the corresponding intra-ZIF concentration in the studied ZIF-71/Torlon MMMs are expected be the same as those in the ZIF-71 bed samples.

**Table 1**
Intra-ZIF liquid sorbate concentrations of *p*-xylene and *o*-xylene in the studied mixture in the ZIF-71 bed samples obtained using $^{13}$C NMR signal analysis at 296 K.

| Sorbate | Sorbate loading (mmol/g)[a] |
|---|---|
| *P*-xylene | 0.56 |
| *O*-xylene | 0.52 |

[a] 20–30% experimental uncertainty.

### 2.4. NMR measurements

$^{13}$C NMR measurements were performed using a wide bore 17.6 T Avance III HD spectrometer (Bruker Biospin) operating at a resonance frequency of 188.6 MHz. For diffusion measurements. $^{13}$C PFG NMR was used instead of $^{1}$H PFG NMR to benefit from the larger $T_2$ NMR relaxation times of $^{13}$C nuclei than $^{1}$H nuclei in the samples studied in this work. The $^{13}$C PFG NMR spectrum of *p*-xylene and *o*-xylene exhibited a single line at around 21 and 20 ppm, respectively, referenced to the sample containing 40% 1,4-dioxane in benzene-$d_6$ (Sigma-Aldrich). Under our conditions of PFG NMR measurements, it was not possible to resolve the spectrum of each isomer in the isomer mixtures.

Magnetic field gradients with sine shapes and strengths up to 23 T/m were generated using *diff50* diffusion probe (Bruker Biospin) at 17.6 T. Duration of magnetic field gradients were chosen between 1 and 2 m s. The total time of diffusion experiments varied between 3 and 6 h with the total number of scans 64–128. The repetition delays were between 8 and 15 s, i.e. at least 1.5 times larger than the respective $T_1$ NMR relaxation time. Samples were kept inside the magnet at the measurement temperature for at least 1 h to ensure sorption equilibrium before performing any NMR measurements. During the NMR measurements, several experiments with identical parameters were repeated after each couple of hours. There was no observed change in the measurement results indicating no change in the intra-ZIF sorbate loading during measurements of each sample that lasted many hours.

The 13-interval PFG NMR pulse sequence with an addition of the eddy current delay was used to perform the diffusion measurements [39,40]. The self-diffusion coefficients ($D$) were acquired by measuring PFG NMR attenuation curves, i.e. normalized area under the PFG NMR signal ($S$) measured as a function of the gradient amplitude ($g$) [33,39,41–44].

$$\Psi = \frac{S(g)}{S(g \approx 0)} = \exp\left( - \frac{< r^2(t) > q^2}{6} \right) = \exp\left(-Dtq^2\right), \quad (1)$$

where $\Psi$ is attenuation of PFG NMR signal, $< r^2 >$ is the mean square displacement (MSD), $q = \gamma g \delta$, $\gamma$ is the gyromagnetic ratio, $\delta$ is the normalized magnetic field gradient durations, and $t$ is the diffusion time as described in Refs. [39,44,45]. For three-dimensional diffusion, MSD is related to $D$ and $t$ by Einstein relation as [33].

$$< r^2(t) >= 6Dt. \quad (2)$$

For two molecular ensembles diffusing with different self-diffusivities, Eq. (1), can be re-written as [33,41,42].

$$\Psi = \frac{S(g)}{S(g \approx 0)} = \sum_{i=1}^{2} p_i \exp\left(-D_i q^2 t\right), \quad (3)$$

where $p_i$ and $D_i$ are population fraction and self-diffusivity of ensemble $i$, respectively. All reported experimental uncertainties in self-diffusivities were estimated by reproducibility of the diffusion data measured with several different PFG NMR samples prepared following an identical procedure.

Longitudinal ($T_1$) and transverse ($T_2$) $^{13}$C NMR relaxation measurements were carried out in the same manner as discussed in Ref. [37] using standard inversion recovery and standard Carr-Purcell-Meiboom-Gill (CPMG) pulse sequences, respectively. In CPMG pulse sequence, tau was equal to 100 μs. The $T_1$ relaxation measurements showed existence of a single $T_1$ NMR relaxation time corresponding to sorbate molecules located inside each NMR sample (Table 2). The results of $T_2$ relaxation measurements exhibited presence of two molecular ensembles with two different $T_2$ NMR relaxation times. In this case, a bi-exponential fitting was used to obtain the values of $T_2$ NMR relaxation times and the corresponding molecular ensemble fractions (Table 2). These fractions were assigned to the molecules located outside of ZIF-71 crystals and/or ZIF-71/Torlon MMMs (ensemble 1) and molecules located inside ZIF crystals (ensemble 2). No intra-polymer $T_2$ ensemble was observed for MMM samples in NMR relaxation measurements. This is in agreement with our previous measurements of liquid molecules in Torlon-based MMM discussed in Ref. [37]. The absence of the intra-polymer component is related to a combination of a low concentration and short $T_2$ times of the studied sorbates in the polymer. All reported NMR studies were performed at 296 K.

**Table 2**
$^{13}$C $T_1$ and $T_2$ NMR relaxation times measured for the studied mixture samples at 17.6 T and 296 K.

| Samples | Sorbate measured by $^{13}$C PFG NMR | $T_1$, s | $T_2$ [1], ms | $T_2$ [2], ms | $p_1$ | $p_2$ |
|---|---|---|---|---|---|---|
| ZIF-71 loaded with *p*-xylene/*o*-xylene mixture | Both | 7.2 | 45 | 11.2 | 0.67 | 0.33 |
| ZIF-71 loaded with *p*-xylene/*o*-xylene mixture | *P*-xylene | 4.8 | 35 | 7.1 | 0.71 | 0.29 |
| ZIF-71 loaded with *p*-xylene/*o*-xylene mixture | *O*-xylene | 6.8 | 34 | 10.5 | 0.68 | 0.32 |
| ZIF-71/Torlon MMM loaded with *p*-xylene/*o*-xylene mixture | Both | 9.7 | 1.4 × $10^3$ | 18.4 | 0.72 | 0.28 |
| ZIF-71/Torlon MMM loaded with *p*-xylene/*o*-xylene mixture | *P*-xylene | 8.7 | 1.4 × $10^3$ | 19.3 | 0.76 | 0.24 |
| ZIF-71/Torlon MMM loaded with *p*-xylene/*o*-xylene mixture | *O*-xylene | 9.4 | 1.0 × $10^3$ | 27.7 | 0.64 | 0.36 |

## 3. Results and discussion

Figs. 1 and 2 show examples of the measured $^{13}$C PFG NMR attenuation curves at 296 K for diffusion of an approximately equimolar mixture of *p*-xylene/*o*-xylene in ZIF-71 crystal beds and ZIF-71/Torlon MMMs, respectively. The data shown in Fig. 1 correspond to the case when only one type of sorbate in the mixture was measured by $^{13}$C PFG NMR because the other isomer in the samples was not $^{13}$C-labeled. Additional diffusion measurements were performed in ZIF-71 crystal beds and ZIF-71/Torlon MMM samples in which both types of sorbates in the mixture were $^{13}$C-labeled. It was observed that the $^{13}$C NMR spectra of both studied isomers consist of a single line at around 20 ppm. As a result, when both isomers in a sample were $^{13}$C-labeled, it was not possible to measure $^{13}$C PFG NMR attenuation curves separately for each isomer. Hence, for these samples, both isomers contributed to the measured $^{13}$C PFG NMR attenuation curves (Fig. 2). The advantage of the measurements of such samples is related to the fact that in this case the diffusion of both types of sorbates were measured in the same sample and at the same time. The latter measurements allowed eliminating an additional experimental uncertainty that might arise in measurements of different samples prepared in an identical manner. As demonstrated below, the observed agreement between the diffusion data obtained under the same conditions with the samples where only one or both xylene isomers together were measured, confirm the reliability and validity of the reported data for each isomer.

It can be seen in Fig. 1 that the PFG NMR attenuation curves deviate from the monoexponential behavior (i.e. the case when all the sorbate molecules diffuse with a single self-diffusivity, as predicted by Eq. (1)). The attenuation curves exhibit a rapid initial decay continued by a slower decay, which indicates the presence of minimum two diffusion ensembles of the same sorbate type with two different self-diffusion coefficients. In all cases, it was observed that Eq. (3), which assumes the existence of two diffusion ensembles, can describe the attenuation curves satisfactorily. In complete analogy with the self-diffusion data

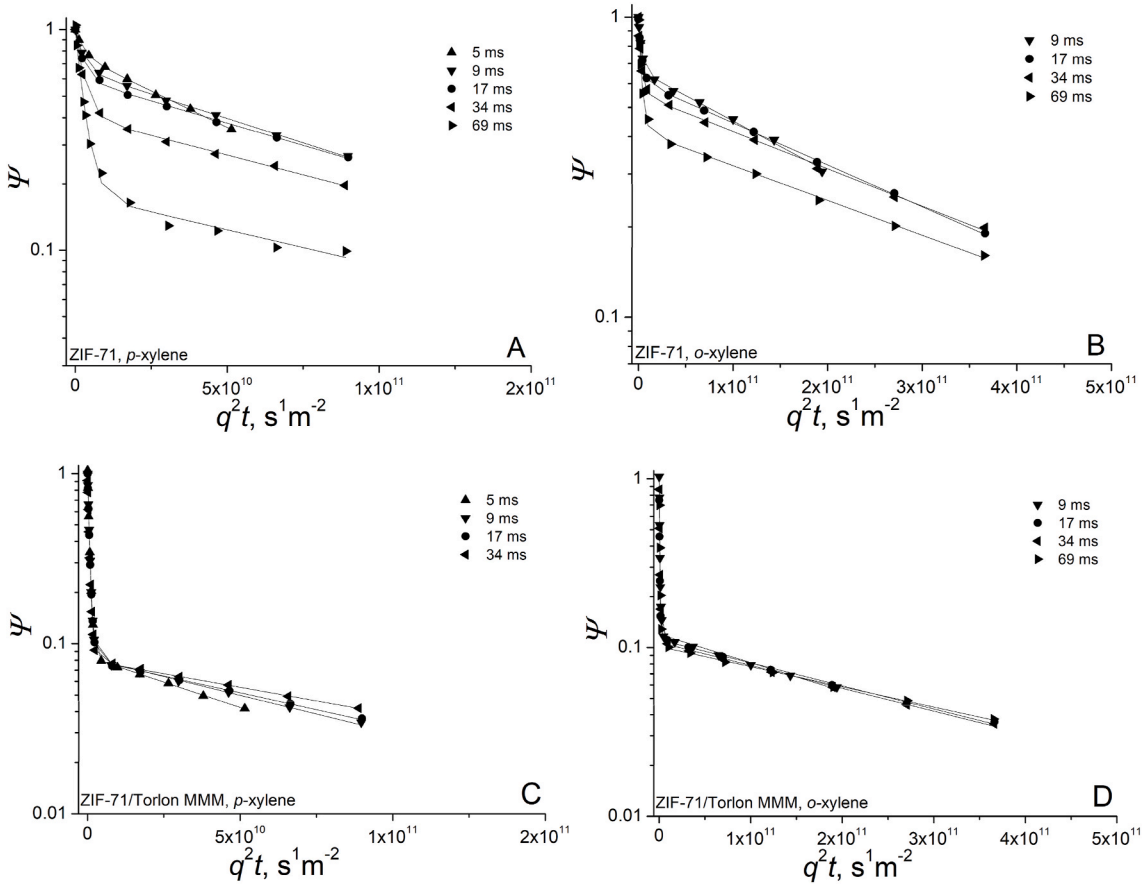


**Fig. 1.** $^{13}$C PFG NMR attenuation curves measured at 296 K in a ZIF-71 crystal bed (A,B) and ZIF-71/Torlon MMM (C,D) loaded with the *p*-xylene/*o*-xylene mixture. Data in A and C corresponds to *p*-xylene diffusion and data in B and D corresponds to *o*-xylene diffusion. The measurements were carried out for different diffusion times shown in the figure. The solid lines represent the results of least-square fitting using Eq. (3). Only one sorbate indicated in the figure was measured by $^{13}$C PFG NMR because only this sorbate was $^{13}$C-labeled.

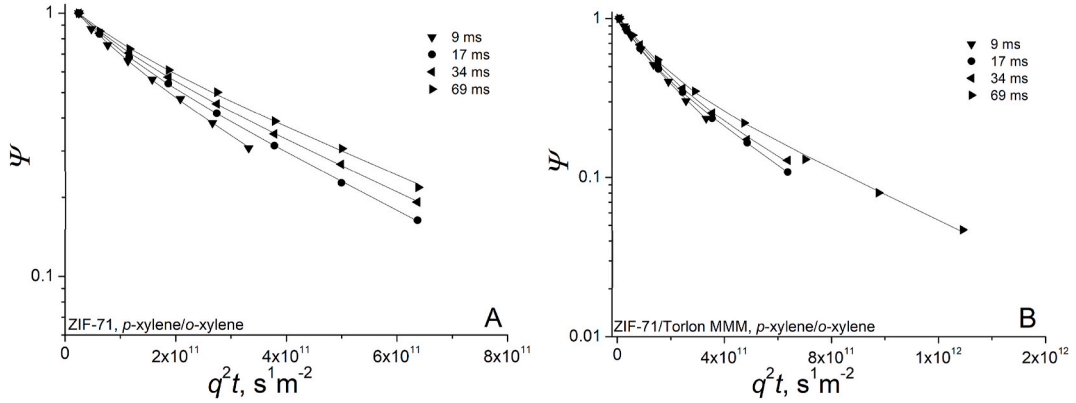


**Fig. 2.** $^{13}$C PFG NMR attenuation curves measured at 296 K in a ZIF-71 crystal bed (A) and ZIF-71/Torlon MMM (B) loaded with the *p*-xylene/*o*-xylene mixture. Both sorbates in the mixture were $^{13}$C-labeled and contributed to the measured curves. The measurements were carried out for different diffusion times shown in the figure. The solid lines represent the results of least-square fitting using Eq. (3).

obtained for single component xylenes discussed in Ref. [37], the faster diffusing ensemble was attributed to sorbate molecules diffusing most of the time outside of the ZIF-71 crystals (for ZIF-71 bed samples) or outside of the MMMs (for the ZIF-71/Torlon MMM samples). At the same time, the slower diffusing ensemble was attributed to the intra-ZIF self-diffusion. No PFG NMR signal corresponding to the intra-polymer self-diffusion was observed for the MMM samples due to short $T_2$ NMR relaxation times combined with small fraction of sorbate molecules in the polymer phase. This observation was found to be in a complete agreement with our previous single component xylenes diffusion data where no PFG NMR signal was observed for the intra-polymer self--diffusion [37].

Similarly, the PFG NMR attenuation curves shown in Fig. 2 deviate from the monoexponential behavior. However, the initial decays of the reported attenuation curves are not as sharp as that seen in Fig. 1. For these curves, the smallest gradient amplitude was chosen to be

sufficiently strong so that all contributions from the faster diffusing ensemble corresponding to the sorbate molecules mostly diffusing outside of ZIF-71 crystals or MMM were attenuated away already at the smallest gradient. This was done to eliminate an additional uncertainty arising from a tri-exponential fitting function (i.e. modified Eq. (3) with three instead of two terms in the right-hand part), which would otherwise be needed for describing the diffusion data. The removal of the contribution from the diffusion outside of ZIF-71 crystals or MMM allowed using Eq. (3) for fitting the PFG NMR diffusion data in Fig. 2. In this case, the two measured ensembles correspond to intra-ZIF diffusion of the two xylene isomers.

Table 3 shows the data for the diffusion of the intra-ZIF ensembles of both isomers. These data results from least square fitting of the measured PFG NMR attenuation curves (Figs. 1 and 2) by Eq. (3). It can be seen from the table that the intra-ZIF self-diffusivities of each sorbate type decreases as the diffusion time and the corresponding root MSD increases. As already discussed in detail in our recent work [37], such behavior is a consequence of an influence of the external crystal surface on the trajectories of the diffusing molecules which reach this surface. Clearly, the intra-crystalline displacements cannot accede the crystal dimensions. This leads to the observed decrease in the measured diffusion coefficients with increasing diffusion time. Such self-diffusivity dependencies can be used to estimate intra-ZIF self-diffusivities $D_0$, which are not influenced by the external crystal surface by applying an analytical relations proposed by Mitra et al. for self-diffusion inside porous spherical particles with radius $R$ [46,47]

$$\frac{D(t)}{D_0} \approx 1 - \frac{f}{3R}\left(\frac{D_0 t}{\pi}\right)^{0.5}, \tag{4}$$

where $f = 4$ and 2, respectively, for the reflecting and adsorbing crystal surfaces. Reflecting boundaries correspond to reflections of diffusing molecules from the crystal external surface. Such reflections can happen due to a lower inside than outside of crystals potential energy of guest molecules and/or presence of clogged pore entrances at the external crystal surface. In the case of adsorbing boundaries, guest molecules with larger displacements have a higher probability to exit the original crystal and stop contributing to the intra-ZIF ensemble. The removal of "fastest" molecules reduces the measured self-diffusivity. Eq. (4) was utilized to fit the measured intra-ZIF self-diffusivity dependencies on diffusion time ($D(t)$) to estimate the $D_0$ values for each studied isomer

**Table 3**
Diffusion data corresponding to the $^{13}$C PFG NMR attenuation curves measured at 296 K for the *p*-xylene/*o*-xylene mixture in ZIF-71 crystal beds and ZIF-71 Torlon MMMs. The root MSDs were calculated by Eq. (2).

| Sample | Sorbate measured by $^{13}$C PFG NMR | Diffusion time (ms) | $D_{p\text{-xylene}}$, $10^{-12}\frac{m^2}{s}$ | Root MSD (*p*-xylene), μm | $D_{o\text{-xylene}}$, $10^{-12}\frac{m^2}{s}$ | Root MSD (*o*-xylene), μm | $p_{p\text{-xylene}}$ | $p_{o\text{-xylene}}$ |
|---|---|---|---|---|---|---|---|---|
| ZIF-71 bed loaded with *p*-xylene/*o*-xylene mixture | Both | 9 | 0.14 ± 0.03 | 0.84 ± 0.08 | 0.031 ± 0.006 | 0.40 ± 0.04 | 0.25 | 0.75 |
| | | 17 | 0.12 ± 0.03 | 1.1 ± 0.1 | 0.025 ± 0.005 | 0.50 ± 0.05 | 0.28 | 0.72 |
| | | 34 | 0.11 ± 0.02 | 1.5 ± 0.2 | 0.023 ± 0.005 | 0.68 ± 0.07 | 0.26 | 0.74 |
| | | 69 | 0.11 ± 0.02 | 2.1 ± 0.2 | 0.021 ± 0.004 | 0.93 ± 0.09 | 0.23 | 0.77 |
| | *P*-xylene | 5 | 0.15 ± 0.04 | 0.70 ± 0.09 | – | – | – | – |
| | | 9 | 0.10 ± 0.03 | 0.8 ± 0.1 | – | – | – | – |
| | | 17 | 0.093 ± 0.023 | 1.0 ± 0.1 | – | – | – | – |
| | | 34 | 0.082 ± 0.021 | 1.3 ± 0.2 | – | – | – | – |
| | | 69 | 0.074 ± 0.019 | 1.8 ± 0.2 | – | – | – | – |
| | *O*-xylene | 9 | – | – | 0.039 ± 0.009 | 0.46 ± 0.06 | – | – |
| | | 17 | – | – | 0.032 ± 0.008 | 0.57 ± 0.07 | – | – |
| | | 34 | – | – | 0.029 ± 0.007 | 0.8 ± 0.1 | – | – |
| | | 69 | – | – | 0.027 ± 0.007 | 1.1 ± 0.1 | – | – |
| ZIF-71/Torlon MMM loaded with *p*-xylene/*o*-xylene mixture | Both | 9 | 0.14 ± 0.03 | 0.84 ± 0.08 | 0.036 ± 0.007 | 0.43 ± 0.04 | 0.28 | 0.72 |
| | | 17 | 0.11 ± 0.02 | 1.1 ± 0.1 | 0.027 ± 0.006 | 0.52 ± 0.05 | 0.41 | 0.59 |
| | | 34 | 0.085 ± 0.017 | 1.3 ± 0.1 | 0.023 ± 0.005 | 0.68 ± 0.07 | 0.50 | 0.50 |
| | | 69 | 0.083 ± 0.017 | 1.9 ± 0.2 | 0.019 ± 0.004 | 0.088 ± 0.09 | 0.52 | 0.48 |
| | *P*-xylene | 5 | 0.14 ± 0.03 | 0.67 ± 0.08 | – | – | – | – |
| | | 9 | 0.10 ± 0.03 | 0.75 ± 0.09 | – | – | – | – |
| | | 17 | 0.091 ± 0.023 | 1.0 ± 0.1 | – | – | – | – |
| | | 34 | 0.073 ± 0.018 | 1.2 ± 0.2 | – | – | – | – |
| | *O*-xylene | 9 | – | – | 0.039 ± 0.010 | 0.46 ± 0.06 | – | – |
| | | 17 | – | – | 0.031 ± 0.008 | 0.57 ± 0.07 | – | – |
| | | 34 | – | – | 0.031 ± 0.008 | 0.8 ± 0.1 | – | – |
| | | 69 | – | – | 0.028 ± 0.007 | 1.1 ± 0.1 | – | – |

and sample (Fig. 3). Due to an existence of a broad distribution over the crystal sizes (Fig. S2) the value of $f$ could not be quantified.

The resulting values of $D_0$ are presented in Fig. 3 and Table 4. These data show that for the same sorbate type there is a consistency, within experimental error, between the $D_0$ values for the ZIF-71 crystal bed and MMM. In complete analogy with the self-diffusion data obtained for single component sorbates discussed in Ref. [37], no effect of ZIF-71 crystal confinement in Torlon polymer was observed on intra-ZIF self-diffusion.

Table 5 lists the ratios of $D_0$ values for the two xylene isomers, viz. diffusion selectivities, obtained for the self-diffusion in the ZIF-71 crystal beds and in the corresponding ZIF-71/Torlon MMMs under the identical or similar conditions. It can be seen in Table 5 that for both the crystal beds and MMMs, the $D_0$ values for smaller *p*-xylene (5.8 Å [48]) are greater by a factor of ~4 than those for larger *o*-xylene (6.8 Å [48]).

Comparison in Table S1 between the values of $D_0$ reported previously for the one-component xylene isomers in Ref. [37] and those presented here for the mixed isomers indicates that replacing about half of molecules of either type of the isomer with the molecules of the other isomer does not change the values of $D_0$, within uncertainty. Similarly, the intra-ZIF self-diffusion selectivities for the *p*-xylene/*o*-xylene mixture (Table 5) were found to be in agreement with the corresponding selectivities obtained for the samples loaded with a single isomer [37]. Separation of mixtures of xylene isomers, which are typically produced in catalytic reforming of crude oil, is a challenging separation owing to the similarity of the properties of these isomers. Clearly, an optimization of this separation using MMMs requires knowledge of diffusion under conditions when more than a single molecular component is present inside membranes. This consideration emphasizes the importance of diffusion studies performed in the current study with the isomer mixture. The reported diffusion selectivity of around 4 for the studied xylene isomer mixture demonstrates promising separation behavior of the considered MMM.

**Table 4**
Intra-ZIF self-diffusivities in the limit of small diffusion times ($D_0$) at 296 K obtained by fitting the PFG NMR data with Eq. (4) for ZIF-71 crystals and ZIF-71/Torlon MMM samples.

| Sample | Sorbate measured by $^{13}$C PFG NMR | $D_{0,\ p\text{-xylene}}$ ($10^{-10}$ m$^2$/s) | $D_{0,\ o\text{-xylene}}$ ($10^{-10}$ m$^2$/s) |
|---|---|---|---|
| ZIF-71 loaded with *p*-xylene/*o*-xylene mixture | *P*-xylene | 0.15 ± 0.04 | – |
| ZIF-71 loaded with *p*-xylene/*o*-xylene mixture | *O*-xylene | – | 0.042 ± 0.011 |
| ZIF-71 loaded with *p*-xylene/*o*-xylene mixture | Both | 0.14 ± 0.03 | 0.034 ± 0.007 |
| ZIF-71/Torlon MMM loaded with *p*-xylene/*o*-xylene mixture | *P*-xylene | 0.16 ± 0.04 | – |
| ZIF-71/Torlon MMM loaded with *p*-xylene/*o*-xylene mixture | *O*-xylene | – | 0.042 ± 0.011 |
| ZIF-71/Torlon MMM loaded with *p*-xylene/*o*-xylene mixture | Both | 0.15 ± 0.03 | 0.041 ± 0.008 |

**Table 5**
Diffusion selectivities, i.e. intra-ZIF self-diffusivity ratios in the limit of small diffusion times ($D_0$), for ZIF-71 crystals and ZIF-71/Torlon MMMs at 296 K.

| Type of mixture | Ratios of $D_0$ values for ZIF-71 beds ($D_{0,ZIF}/D_{0,ZIF}$) | Ratios of $D_0$ values for ZIF-71/Torlon MMMs ($D_{0,MMM}/D_{0,MMM}$) |
|---|---|---|
| *P*-xylene/*o*-xylene[a] | 3.6[c] | 3.8[c] |
| *P*-xylene/*o*-xylene[b] | 4.1[d] | 3.7[d] |

[a] Only one sorbate in each mixture sample was $^{13}$C-labeled and measured by $^{13}$C PFG NMR.
[b] Both sorbates in the mixture sample were $^{13}$C-labeled and measured by $^{13}$C PFG NMR.
[c] 40% experimental uncertainty.
[d] 30% experimental uncertainty.

## 4. Conclusion

$^{13}$C PFG NMR was used to study diffusion of an approximately equimolar mixture of *p*-xylene and *o*-xylene inside ZIF-71/Torlon MMM and in the reference samples of ZIF-71 crystal beds. It was observed that the intra-ZIF self-diffusivities in ZIF-71/Torlon MMMs and the corresponding ZIF crystal beds decrease with increasing diffusion time. The dependencies of self-diffusivities were explained by the effects at the external crystal surface arising from restrictions of the intra-ZIF diffusion displacements by the ZIF-71 crystal sizes. Using a well-established approach, the measured time dependencies of the intra-ZIF self-diffusivities were utilized to obtain the intra-ZIF self-diffusivities ($D_0$), which were not perturbed by the influence of the external crystal surface. Under the same or similar experimental conditions, the values of $D_0$, within uncertainty, were found to be the same in ZIF-71/Torlon MMMs and in the corresponding ZIF beds for each type of sorbate used. In complete analogy with the self-diffusion data obtained for single component xylenes discussed in our recent work [37], no influence of

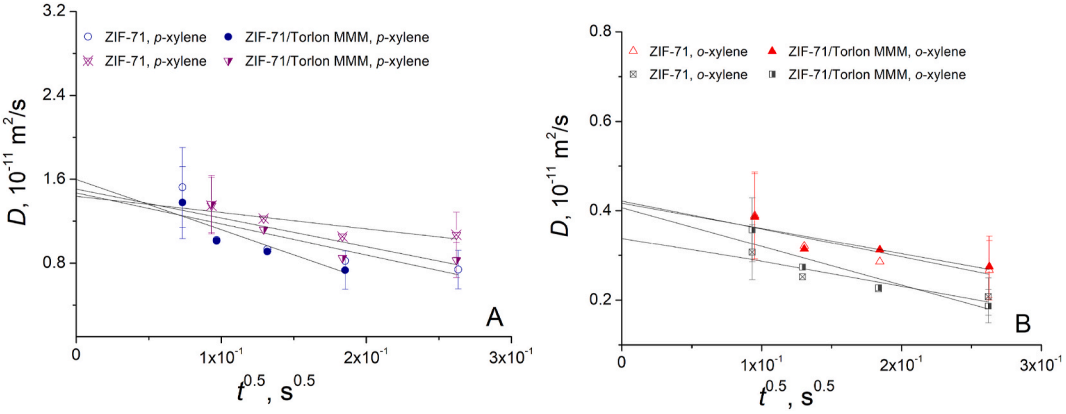


**Fig. 3.** Self-diffusivities at 296 K for *p*-xylene (A) and *o*-xylene (B) plotted as a function of $t^{0.5}$ for the studied ZIF-71 crystal beds (empty symbols and empty symbols with crosses) and ZIF-71/Torlon MMM (filled symbols and half-filled symbols) samples loaded with the *p*-xylene/*o*-xylene mixture. The solid lines represent results of least-square fitting using Eq. (4). The data were measured by the 13-interval PFG NMR pulse sequence at 17.6 T. Hollow symbols with crosses and half-filled symbols correspond to the samples where both sorbates were measured by $^{13}$C PFG NMR. All other symbols correspond to the measurements were only a single sorbate was measured.

the ZIF-71 crystal confinement in Torlon polymer on intra-ZIF self--diffusion of the studied mixture was observed. The intra-ZIF diffusion selectivity for the diffusion of the mixture of the xylene isomers in the MMM was found to be about 4, which shows promise of the studied membranes in the separation applications. To our knowledge, this work represents the first direct quantification of a diffusion selectivity for mixed liquids inside filler particles of MMMs.

## CRediT authorship contribution statement

**Amineh Baniani:** Investigation, Writing – original draft, Writing – review & editing. **Matthew P. Rivera:** Investigation, Writing – review & editing. **Ryan P. Lively:** Funding acquisition, Investigation, Writing – review & editing. **Sergey Vasenkov:** Writing – review & editing, Project administration, Investigation, Funding acquisition.

## Declaration of competing interest

The authors declare that they have no known competing financial interests or personal relationships that could have appeared to influence the work reported in this paper.

## Acknowledgments

This work was financially supported by NSF (CBET awards No. 1836735 and No. 1836738). A portion of this work was carried out in the McKnight Brain Institute at the National High Magnetic Field Laboratory's AMRIS Facility, which is supported by National Science Foundation Cooperative Agreement No. DMR-1157490

and the State of Florida. This work was supported in part by an NIH award, S10RR031637, for magnetic resonance instrumentation.

## Appendix A. Supplementary data

Supplementary data to this article can be found online at https://doi.org/10.1016/j.micromeso.2022.111960.

## References

[1] M.A. Aroon, A.F. Ismail, T. Matsuura, M.M. Montazer-Rahmati, Performance studies of mixed matrix membranes for gas separation: a review, Separ. Purif. Technol. 75 (2010) 229–242.
[2] P.S. Goh, A.F. Ismail, S.M. Sanip, B.C. Ng, M. Aziza, Recent advances of inorganic fillers in mixed matrix membrane for gas separation, Separ. Purif. Technol. (2011) 81.
[3] Y. Cheng, Y. Ying, L. Zhai, G. Liu, J. Dong, Y. Wang, M.P. Christopher, S. Long, Y. Wang, D. Zhao, Mixed matrix membranes containing MOF@COF hybrid fillers for efficient $CO_2/CH_4$ separation, J. Membr. Sci. 573 (2019) 97–106.
[4] N. Tien-Binh, H. Vinh-Thang, X.Y. Chen, D. Rodrigue, S. Kaliaguine, Polymer functionalization to enhance interface quality of mixed matrix membranes for high $CO_2/CH_4$ gas separation, J. Mater. Chem. 3 (2015) 15202–15213.
[5] A.L. Ahmad, Z.A. Jawad, S.C. Low, S.H.S. Zein, A cellulose acetate/multi-walled carbon nanotube mixed matrix membrane for $CO_2/N_2$ separation, J. Membr. Sci. 451 (2014) 55–66.
[6] Q. Li, Q. Liu, J. Zhao, Y. Hua, J. Sun, J. Duan, W. Jin, High efficient water/ethanol separation by a mixed matrix membrane incorporating MOF filler with high water adsorption capacity, J. Membr. Sci. 544 (2017) 68–78.
[7] W. Li, S.A.S.C. Samarasinghe, Tae-HyunBae, enhancing $CO_2/CH_4$ separation performance and mechanical strength of mixed-matrix membrane via combined use of graphene oxide and ZIF-8, J. Ind. Eng. Chem. 67 (2018) 156–163.
[8] S. Quan, S.W. Li, Y.C. Xiao, L. Shao, $CO_2$-Selective mixed matrix membranes (MMMs) containing graphene oxide (GO) for enhancing sustainable $CO_2$ capture, Int. J. Greenh. Gas Control 56 (2017) 22–29.
[9] R.T. Adams, J.S. Lee, T.-H. Bae, J.K. Ward, J.R. Johnson, C.W. Jones, S. Nair, W. J. Koros, $CO_2$–$CH_4$ permeation in high zeolite 4A loading mixed matrix membranes, J. Membr. Sci. 367 (2011) 197–203.
[10] M.S. Boroglu, A.B. Yumru, Gas separation performance of 6FDA-DAM-ZIF-11 mixed-matrix membranes for $H_2/CH_4$ and $CO_2/CH_4$ separation, Separ. Purif. Technol. 173 (2017) 269–279.
[11] R.C. Dutta, S.K. Bhatia, Interfacial engineering of MOF-based mixed matrix membrane through atomistic simulations, J. Phys. Chem. C 124 (2020) 594–604.
[12] L. Diestel, N. Wang, B. Schwiedland, F. Steinbach, U. Giese, J. Caro, MOF based MMMs with enhanced selectivity due to hindered linker distortion, J. Membr. Sci. 492 (2015) 181–186.
[13] B.R. Pimentel, A. Parulkar, E.-k. Zhou, N.A. Brunelli, R.P. Lively, Zeolitic imidazolate frameworks: next-generation materials for energy-efficient gas separations, Chemistry & Sustainability Energy & Materials 7 (2014) 3202–3240.
[14] P.A. Banerjee R, B. Wang, C. Knobler, H. Furukawa, M. O'Keeffe, O.M. Yaghi, High-throughput synthesis of zeolitic imidazolate frameworks and application to CO2 capture, Science 319 (2008) 939–943.
[15] K.S. Park, Z. Ni, A.P. Côté, J.Y. Choi, R. Huang, F.J. Uribe-Romo, H.K. Chae, M. O'Keeffe, O.M. Yaghi, Exceptional chemical and thermal stability of zeolitic imidazolate frameworks, Proc. Natl. Acad. Sci. Unit. States Am. 103 (2006) 10186–10191.
[16] C. Zhang, Y. Dai, J.R. Johnson, O. Karvan, W.J. Koros, High performance ZIF-8/6FDA-DAM mixed matrix membrane for propylene/propane separations, J. Membr. Sci. 389 (2012) 34–42.
[17] H. An, K.Y. Cho, S. Back, X.H. Do, J.-D. Jeon, H.K. Lee, K.-Y. Baek, J.S. Lee, The significance of the interfacial interaction in mixed matrix membranes for enhanced propylene/propane separation performance and plasticization resistance, Separ. Purif. Technol. (2021) 261.
[18] T.-H. Bae, J.S. Lee, W. Qiu, W.J. Koros, C.W. Jones, S. Nair, A high-performance gas-separation membrane containing submicrometer-sized metal-organic framwork crystals, Angew. Chem. Int. Ed. 49 (2010) 9863–9866.
[19] J. Sánchez-Laínez, B. Zornoza, Á. Mayoral, Á. Berenguer-Murcia, Diego Cazorla-Amorós, C. Téllez, J. Coronas, Beyond the $H_2/CO_2$ upper bound: one-step crystallization and separation of nano-sized ZIF-11 by centrifugation and its application in mixed matrix membranes, J. Mater. Chem. 3 (2015) 6549–6556.
[20] S. Sorribas, P. Gorgojo, C. Téllez, J. Coronas, A.G. Livingston, High flux thin film nanocomposite membranes based on metal–organic frameworks for organic solvent nanofiltration, J. Am. Chem. Soc. 135 (2013) 15201–15208.
[21] G.M. Shi, T. Yang, T.S. Chung, Polybenzimidazole (PBI)/Zeolitic imidazolate frameworks (ZIF-8) mixed matrix membranes for pervaporation dehydration of alcohols, J. Membr. Sci. 415–416 (2012) 577–586.
[22] S. Basu, M. Maes, A. Cano-Odena, L. Alaerts, D.E.D. Vos, I.F.J. Vankelecom, Solvent resistant nanofiltration (SRNF) membranes based on metal-organic frameworks, J. Membr. Sci. 344 (2009) 190–198.
[23] M.M.H.S. Buddin, A.L. Ahmad, A review on metal-organic frameworks as filler in mixed matrix membrane: recent strategies to surpass upper bound for $CO_2$ separation, J. $CO_2$ Util. 51 (2021), 101616.
[24] M.v. Essen, R. Thür, L.v.d. Akker, M. Houben, I.F.J. Vankelecom, K. Nijmeijer, Z. Borneman, Tailoring the separation performance of ZIF-based mixed matrix membranes by MOF-matrix interfacial compatibilization, J. Membr. Sci. 637 (2021), 119642.
[25] H. Yin, C.Y. Lau, M. Rozowski, C. Howard, Y. Xu, T. Lai, M.E. Dose, R.P. Lively, M. L. Lind, Free-standing ZIF-71/PDMS nanocomposite membranes for the recovery of ethanol and 1-butanol from water through pervaporation, J. Membr. Sci. 529 (2017) 286–292.
[26] Y. Li, L.H. Wee, J.A. Martens, I.F.J. Vankelecom, ZIF-71 as a potential filler to prepare pervaporation membranes for bio-alcohol recovery, J. Mater. Chem. 2 (2014) 10034–10040.
[27] S. Liu, G. Liu, X. Zhao, W. Jin, Hydrophobic-ZIF-71 filled PEBA mixed matrix membranes for recovery of biobutanol via pervaporation, J. Membr. Sci. 446 (2013) 181–188.
[28] E.M. Forman, A. Baniani, L. Fan, K.J. Ziegler, E. Zhou, F. Zhang, R.P. Lively, S. Vasenkov, Ethylene diffusion in crystals of zeolitic imidazole framework-11 embedded in polymers to form mixed-matrix membranes, Microporous Mesoporous Mater. 274 (2019) 163–170.
[29] E.M. Forman, A. Baniani, L. Fan, K.J. Ziegler, E. Zhou, F. Zhang, R.P. Lively, S. Vasenkov, Relationship between ethane and ethylene diffusion inside ZIF-11 crystals confined in polymers to form mixed-matrix membranes, J. Membr. Sci. 593 (2020).
[30] A. Baniani, S.J. Berens, M.P. Rivera, R.P. Lively, S. Vasenkov, Potentials and Challenges of High-Field PFG NMR Diffusion Studies with Sorbates in Nanoporous Media, 2021. Adsorption.
[31] R. Mueller, S. Zhang, C. Zhang, R.P. Lively, S. Vasenkov, Relationship between long-range diffusion and diffusion in the ZIF-8 and polymer phases of mixed-matrix membrane by high field NMR diffusometry, J. Membr. Sci. 477 (2015) 123–130.
[32] R. Mueller, V. Hariharan, C. Zhang, R. Lively, S. Vasenkov, Relationship between mixed and pure gas self-diffusion for ethane and ethene in ZIF-8/6FDA-DAM mixed-matrix membrane by pulsed field gradient NMR, J. Membr. Sci. 499 (2016) 12–19.
[33] J. Kärger, D.M. Ruthven, D.N. Theodorou, Diffusion in Nanoporous Materials, Wiley-VCH Verlag GmbH & Co. KGaA, Weinheim, Germany, 2012.
[34] C. Chmelik, J. Kärger, Imaging of transient guest profiles in nanoporous host materials: a new experimental technique to study intra-crystalline diffusion, Adsorption 16 (2010) 515–523.
[35] A. Baniani, C. Chmelik, E.M. Forman, L. Fan, K.J. Ziegler, E. Zhou, F. Zhang, R. Lyndon, R.P. Lively, S. Vasenkov, Anomalous relationship between molecular size and diffusivity of ethane and ethylene inside crystals of zeolitic imidazolate framework-11, J. Phys. Chem. C 123 (2019) 16813–16822.
[36] S. Berens, C. Chmelik, F. Hillman, J. Kärger, H.-K. Jeongc, S. Vasenkov, Ethane diffusion in mixed linker zeolitic imidazolate framework-7-8 by pulsed field gradient NMR in combination with single crystal IR microscopy, Phys. Chem. Chem. Phys. 20 (2018) 23967–23975.
[37] A. Baniani, M.P. Rivera, R.P. Lively, S. Vasenkov, Quantifying diffusion of organic liquids in a MOF component of MOF/polymer mixed-matrix membranes by high field NMR, J. Membr. Sci. 640 (2021), 119786.

[38] R.P. Lively, M.E. Dose, J.A. Thompson, B.A. McCool, R.R. Chance, W.J. Koros, Ethanol and water adsorption in methanol-derived ZIF-71, Chem. Commun. 47 (2011) 8667–8669.
[39] R.M. Cotts, M.J.R. Hoch, T. Sun, J.T. Markert, Pulsed field gradient stimulated echo methods for improved NMR diffusion measurements in heterogeneous systems, J. Magn. Reson. 83 (1989) 252–266.
[40] S.J. Gibbs, C.S. Johnson, A PFG NMR experiment for accurate diffusion and flow studies in the presence of eddy currents, J. Magn. Reson. 93 (1991) 395–402.
[41] J. Kärger, H. Pfeifer, W. Heink, Principles and application of self-diffusion measurements by NMR, Adv. Magn. Reson. 12 (1988) 1–89.
[42] J. Kärger, M. Avramovska, D. Freude, J. Haase, S. Hwang, R. Valiullin, Pulsed Field Gradient NMR Diffusion Measurement in Nanoporous Materials, Adsorption, 2020.
[43] P.T. Callaghan, D. MacGowan, K.J. Packer, F.O. Zelaya, Influence of field gradient strength in NMR studies of diffusion in porous media, Magn. Reson. Imaging 9 (1991) 663–671.
[44] E.O. Stejskal, J.E. Tanner, Spin diffusion measurements: spin echoes in the presence of a time-dependent field gradient, J. Chem. Phys. 42 (1965) 288–292.
[45] P. Galvosas, F. Stallmach, G. Seiffert, J. Kärger, U. Kaess, G. Majer, Generation and application of ultra-high-intensity magnetic field gradient pulses for NMR spectroscopy, J. Magn. Reson. 151 (2001) 260–268.
[46] P.P. Mitra, P.N. Sen, Effects of microgeometry and surface relaxation on NMR pulsed-field-gradient experiments: simple pore geometries, Phys. Rev. B 45 (1992) 143–156.
[47] P.P. Mitra, P.N. Sen, L.M. Schwartz, Short-time behavior of the diffusion coefficient as a geometrical probe of porous media, Phys. Rev. B 47 (1993) 8565–8574.
[48] J.-R. Li, R.J. Kuppler, H.-C. Zhou, Selective gas adsorption and separation in metal–organic frameworks, Chem. Soc. Rev. 38 (2009) 1477–1504.